Resistance of Concrete With Various Types of Coarse Aggregate to Coupled Effects of Thermal Shocks and Chemicals

Muhammad Monowar Hossain , Safat Al-Deen , Sukanta Kumer Shill * , Md Kamrul Hassan

Posted Date: 12 December 2023

doi: 10.20944/preprints202312.0767.v1

Keywords: lightweight aggregate; spalling; residual strength; thermal properties; microstructure

Article

Resistance of Concrete with Various Types of Coarse Aggregate to Coupled Effects of Thermal Shocks and Chemicals

Muhammad Monowar Hossain [a,b], Safat Al-Deen [a,*], Sukanta Kumer Shill [a] and Md Kamrul Hassan [a]

[a] School of Engineering and Information Technology, UNSW, Australia.
[b] Department of Civil Engineering, Military Institute of Science and Technology, Bangladesh.
* Correspondence: s.al-deen@unsw.edu.au

Abstract: Rigid pavements at military airfields experience surface deterioration within 6-18 months of construction. The cause of this degradation is mainly due to combined exposure to repeated heat shocks from jet engine exhaust and spilled aviation oils (hydrocarbons). Surface degradation occurs in the form of disintegration of aggregates and cement paste into small pieces that pose severe risks of physical injury to maintenance crews or damage to an aircraft engine. Since coarse aggregates typically occupy 60-80% of the concrete volume, aggregates' thermal properties and microstructure should play a crucial role in the degrading mechanism. At high temperatures, concrete with lightweight aggregates is reported to have better performance compared to concrete with normal-weight aggregate. Thus, the present study carried out a detailed investigation of the mechanical and thermal performance of lightweight aggregate concrete exposed to the combined effects of high temperature and hydrocarbon oils simultaneously. To identify the resistance of different concrete with various lightweight coarse aggregates, pumice, perlite, lytag (sintered fly ash), and crushed brick were used as lightweight coarse aggregates in concrete. Also, basalt aggregate concrete was used as a reference. After cyclic exposures, all specimens were tested for residual mechanical, thermal, chemical, and microstructural properties. Overall, concrete with crushed brick aggregate and LYTAG used in this study showed superior resistance to the simulated airfield conditions.

Keywords: lightweight aggregate; spalling; residual strength; thermal properties; microstructure

1. Introduction

In concrete technology, coarse aggregates with a bulk density lower than 2000 kg/m^3 are usually considered lightweight aggregates (LWA) [1]. Nowadays, LWA is an essential construction material to produce lightweight concrete for many applications in civil engineering industries. To produce lightweight aggregate concrete (LWAC), lightweight fine aggregate and lightweight coarse aggregate could be used combined or normal fine aggregate could be used with LWA.

There are two types of LWA: artificial and natural. Rapid cooling of volcanic magma forms the natural LWA; thus, its appearance and internal pore structure vary, making it difficult to control quality. A few examples of natural LWA include pumice, volcanic scoria, diatomite, sawdust, bottom ash, and starch-based aggregate. Besides, artificially made LWA include perlite, slate, lytag (sintered fly ash), expanded shale, vermiculite, and bonded fly ash. Crushed bricks are also used as LWA as they resemble sintered clay aggregate and possess better thermal properties [2]. Since natural LWA are found in abundance in some regions of the world, their use in LWAC can significantly reduce the cost.

The key characteristics of LWA are low density, higher porosity, good thermal properties, and better fire resistance [3-5]. As stated, LWAC used in structural elements has its inherent benefits of lower thermal coefficient and thermal expansion, higher strength-to-weight ratio, and better tensile strain capacity due to air voids in the LWA [1, 6]. Over the last few decades, many countries adopted

 doi:10.20944/preprints202312.0767.v1

LWAC to build bridges and houses, such as the Prudential Life Building (42-story) in Chicago, the 50-story Australia Square Tower, and large-span bridges in Norway.

Fire's adverse effect on concrete's mechanical properties has been extensively studied throughout the 20th century [7, 8]. Although aggregate is an inert material, it occupies 60-80% of the volume and influences thermal, dimensional stability and elastic properties of concrete. The compressive strength of the LWA highly influences the compressive strength of LWAC. Mineralogical properties of aggregate, such as shape, texture, moisture content, specific gravity and bulk unit weight also influence concrete mechanical properties. Thus, aggregate has a tangible impact on the phenomena once exposed to higher temperatures [9]. In the past, many researchers suggested that the addition of supplementary binding materials, such as fly ash, slag, silica fume, and metakaolin, increases the durability of LWAC [10]. However, a few other research pieces indicated that silica fume or other supplementary materials might enhance concrete density, resulting in explosive spalling due to increased pore pressure at elevated temperatures [7].

Rigid pavements at military airbases are usually constructed using Portland cement concrete (PCC) [13]. Rigid pavements at military airbases face extremely harsh operating conditions [14-16]. In the early 1980s, after the induction of F/A-18 aircraft, rigid pavement has been experiencing rapid pavement surface damage issues worldwide [13, 17-19]. Modern military aircraft's hot exhaust from auxiliary power units (APUs) and aviation oils spill either in conjunction or separately affecting the performance of the pavement [13]. APU exhaust hit the ground at 45^0 angles, and the maximum temperature of the surface was recorded to reach 175°C after an average exposure of 15 minutes [11, 20]. Figure 1 shows the heat map of airfield pavement exposed to the exhaust of an F/A-18 Hornet aircraft. The combined effects of the aviation oil spill and elevated temperature cause surface spalling at airfield pavements. Spalling produces foreign object debris (FOD) in the airfield as small pieces of concrete and aggregates are peeled off from the surface of the pavement. As reported [11], these FODs pose safety hazards to maintenance crews or severe damage to aircraft engines if sucked in. Depending on the amount of FOD, military airfields may even be declared non-operational and, thus, require quick repair/maintenance.

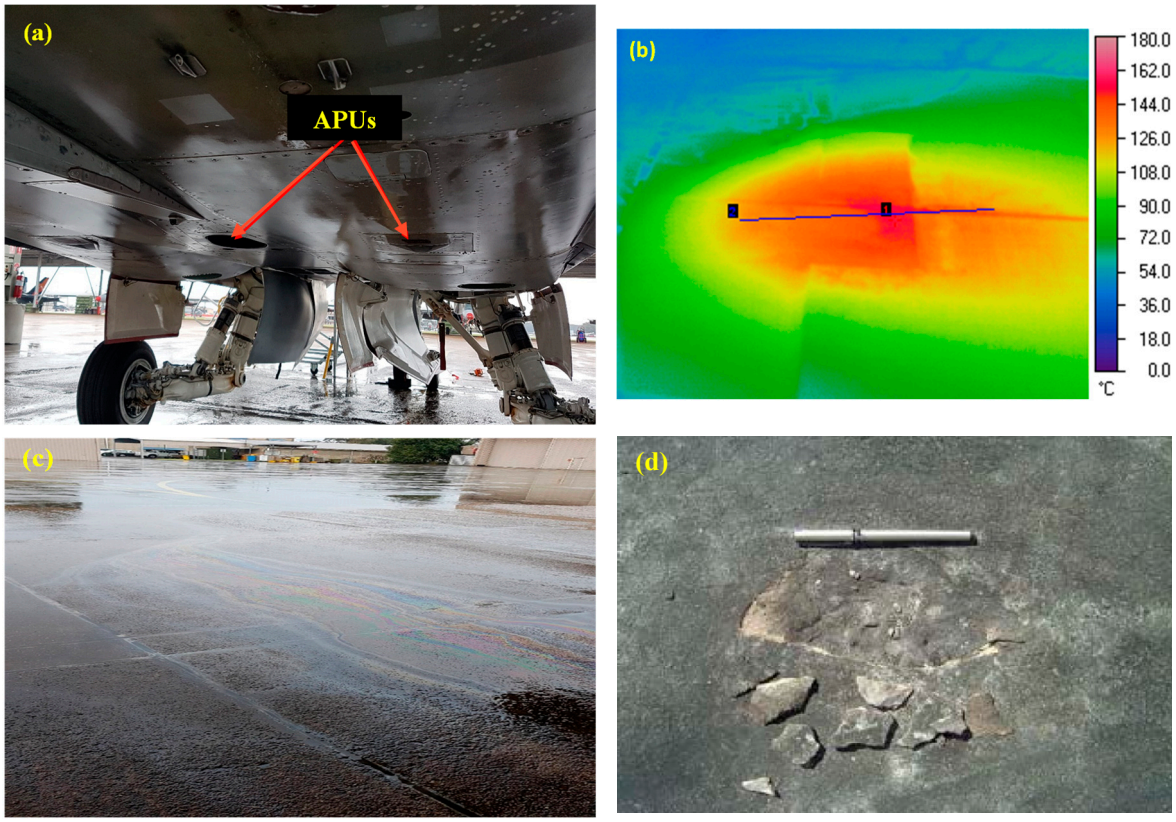

 doi:10.20944/preprints202312.0767.v1

Figure 1. (a) APUs of F/A-18 [11], (b) Heat map of concrete pavement exposed to APU exhaust, (c) Pavement soaked with oils after single maintenance, (d) Spalling of pavement [11, 12].

This study investigates the influence of LWA on spalling resistance of concrete repeatedly exposed to simulated airbase conditions. Although some studies on the performance of lightweight aggregate concrete exposed to high to very high temperatures are available [9, 21], none of the previous studies investigated the combined effects of chemicals and high temperatures on the durability of LWAC. Based on the comprehensive research, residual mechanical and thermal properties, and spalling behaviour of LWAC are reported. It can be noted that this study will facilitate in selecting the suitable coarse aggregate type for military airfield pavement construction to minimize surface spalling.

Four different lightweight aggregates, such as pumice, perlite, lytag, and crushed brick were chosen to produce concrete specimens for this experimental investigation. Ordinary Portland cement (OPC) was used as a binder for each coarse aggregate type. A set of concrete specimens with basalt aggregate was prepared as the benchmark. The residual mechanical properties of the exposed concrete in terms of indirect tensile strength, stress-strain behaviour, compressive strength, spalling, thermal properties, and microstructural conditions were evaluated and revealed in the present study.

2. Experimental Program

2.1. Materials

Australian general-purpose cement (AS 3972) was used for the preparation of concrete specimens [22]. Table *1* shows the chemical analysis of LWA obtained by the XRF analysis. River sand (fineness modulus of 2.60) was used as a fine aggregate. The specific gravity and the water absorption capacity of sand were 2.62 and 0.54%, respectively. Local coarse aggregate (basalt) of a maximum of 10 mm size was used for preparing control concrete specimens. The water absorption capacity, specific gravity, and dry-rodded unit weight of basalt were 0.34%, 2.66 and 1500 kg/m^3, respectively. Pumice, perlite, lytag (PFA based) and crushed brick were used for preparing the LWAC samples, as shown in Figure 2. Ordinary tap water was used to cast concrete samples. ADVA 650 super plasticiser, which is a modified synthetic carboxylated polymer, was used to enhance the workability of concrete.

Table 1. Qualitative XRF chemical analysis of lightweight aggregate and cement.

Chemical analysis (% by mass)	Pumice	Perlite	Lytag	Brick	Basalt	White Gravel	River Gravel	Peach Stone	Portland cement	GPC
Calcium oxide (CaO)	3.37	2.14	3.44	8.095	4.64	-	0.26	-	64.5	4.29
Silica (SiO_2)	71.41	75.64	41.35	56.67	58.24	97.25	88.89	93.66	20.20	60.06
Alumina (Al_2O_3)	10.46	10.91	20.89	11.76	15.72		4.27	2.47	4.8	17.52
Iron oxide (Fe_2O_3)	6.70	2.81	23.54	15.03	9.79	1.46	3.98	2.724	3.1	10.68
Sulphur trioxide (SO_3)	0.86	0.81	1.09	0.44	0.668	1.13	3.982	1.02	2.70	0.901

Preprints (www.preprints.org) | NOT PEER-REVIEWED | Posted: 12 December 2023 doi:10.20944/preprints202312.0767.v1

Magnesia (MnO)	0.21	0.22	0.152	0.30	0.137	-	-	-	1.20	0.228
Titanium oxide (TiO_2)	0.65	-	1.17	1.07	1.09	-	0.265	-	0.52	2.15
Potassium Oxide (K_2O)	6.00	7.40	5.59	5.68	9.13	-	1.168	-	0.67	3.56
Specific Gravity	1.5	0.30	2.10		2.66	-	-	-	-	-
Moisture %	45	35	15	12.5	4.3	-	-	-	-	-

2.2. Concrete mixing and specimen preparation

The mix ratio of the control and LWAC specimens is presented in Table 2. For mixing and compaction, a rotary drum mixer machine and tabletop vibrator were used. LWAs were pre-soaked to maintain the desired level of workability. Samples were cured in a fog room for four weeks at 23 ± 1 °C temperature with relative humidity (RH) > 90%. Cylinder specimens (100 mm x 200 mm) were cast to determine the residual mechanical properties. After 28 days of fog room curing, initial mechanical and thermal properties tests were conducted. All other residual tests were conducted after every 20 times of exposures to the conditions. In all cases, an average of three samples of data was recorded.

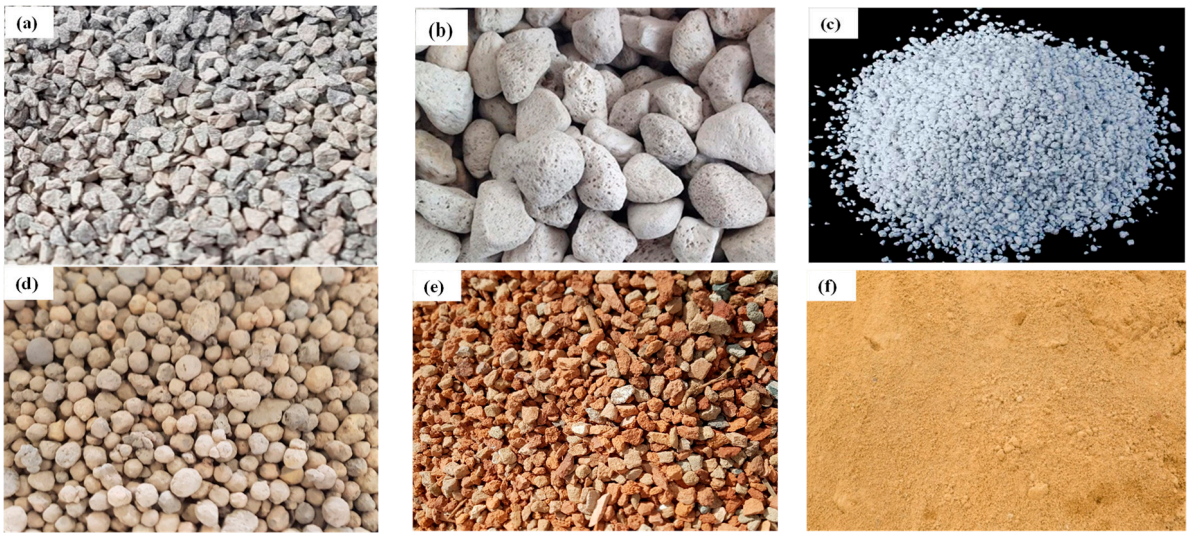

Figure 2. Types of coarse and fine aggregates: (a) Basalt, (b) Pumice, (c) Perlite, (d) Lytag, (e) Brick chips and (f) River sand.

Table 2. Mix design of concrete and dry unit weight of the samples.

Designation of mixture	Cement (kg/m³)	Sand (kg/m³)	Coarse Aggregate (kg/m³)	*W/C ratio*	Super plasticizer (kg/m³)	Dry unit weight of concrete (kg/m³)
Control	462	792	1012	0.45	0	2323

Preprints (www.preprints.org) | NOT PEER-REVIEWED | Posted: 12 December 2023 doi:10.20944/preprints202312.0767.v1

Designation of mixture	Cement (kg/m³)	Sand (kg/m³)	Coarse Aggregate (kg/m³)	*W/C ratio*	Super plasticizer (kg/m³)	Dry unit weight of concrete (kg/m³)
Pumice	462	714	368	0.45	1.0	1897
Perlite	320	714	407	0.37	5.0	1578
Lytag	280	800	835	0.45	4.8	1909
Crushed Brick	462	750	1035	0.45	3.0	2094

2.3. Thermal and chemical (HC fluids) exposures

Concrete samples were repeatedly exposed to high temperatures only and were exposed to the coupled effect of HC fluids and high-temperature cycles simultaneously. As reported, [11, 13, 17, 18] military airfield pavements are often soaked with different aviation oils such as aviation fuel, hydraulic oil, and engine oil. Therefore, in this experiment, jet fuel (F-34 kerosene grade), AeroShell Fluid 31 and AeroShell Turbine Oil 500 were procured and mixed in a 1:1:1 ratio and sprayed on the concrete specimens. For thermal exposure, concrete samples were heated in an electric oven at 175^{0}C temperature for 15 minutes [11]. Figure 3 shows the duration of a thermal cycle used in the study. After the heat exposures, concrete samples were kept outdoors to cool down to ambient temperature. Moreover, water was sprayed on the surface of the concrete samples once a week to simulate rainfall effects on the samples. Oil spraying, heating and cooling were cyclically carried out until surface spalling occurred. Concrete samples were exposed to aviation oils and high thermal cycles daily except weekends over the 4-6 months. The notation 0, 20, 40, 60 and 80 denotes the number of high temperatures or combined high temperature and HC fluids exposure as mentioned in the individual cases.

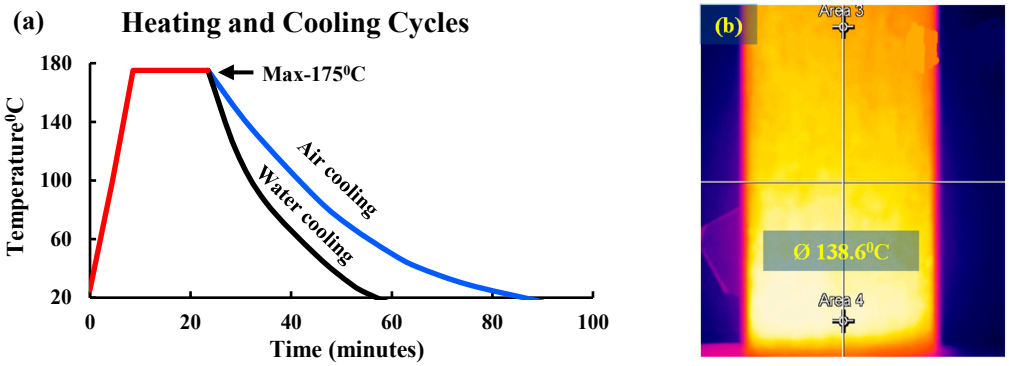

Figure 3. (a) Heating and cooling cycle for specimens, (b) Heat map of the sample during air cooling.

2.4. Tests

2.4.1. Residual mechanical properties test

As per AS 1012.9-2014 [23], LWAC samples were tested for initial and residual compressive strength at intervals of 20 cycles. A universal hydraulic testing machine was used to determine the compressive strength of concrete with a loading rate of 0.3 MPa/s.

2.4.2. Stress-strain test

 doi:10.20944/preprints202312.0767.v1

Techno test (manufacturer) compression testing machine having closed-loop, servo-controlled with a capacity of 3000 KN was used for the stress-strain test. A compressor meter with two displacement transducers with a gauge length of 100 mm was directly attached to the test sample to monitor strain. For each specimen, the displacement between the machine plates was also monitored. During the test, the strain rate of 0.07 mm/min was maintained.

2.4.3. Determination of Thermal Properties.

The specimens' specific heat and thermal conductivity were measured after 0, 40, 60 and 80 cycles of exposures. As per ASTM C518 [24], Netzsch (manufacturer) Lambda 446 heat flow machine was used to test 150 mm x 150 mm x 25 mm size samples for specific heat and thermal conductivity. While measuring the specimen's thermal properties, a 20°C temperature gradient difference between the two plates was maintained. Two heat flow sensors were attached to the plates to measure the heat flow into the material and out of the material.

2.4.4. Fourier transform infrared spectroscopy (FTIR) analysis

For FTIR analysis, samples were taken from the top surface up to a depth of 25 mm, which previous researchers reported as the maximum spalling depth [13, 17]. A ball mill machine was used to pulverise the collected samples. Then the FTIR spectrum of each powder sample was obtained. Before each scanning, the background spectrum of the laboratory environment was scanned. The spectrum of all samples was obtained by 16 scans of wavelength between 3800 cm^{-1} to 650 cm^{-1} using the resolution of 4 cm^{-1}. Spectrums were analysed to understand different covalent bonds, functioning groups, and decomposition of compounds.

2.4.5. Thermogravimetric (TG) and differential scanning calorimetry (DSC) analysis

DSC and TG tests were conducted after 0, 40, and 80 cycles of HC fluids and high-temperature exposures. Concrete samples were crushed, milled, and sieved beforehand. NETZSCH STA 449C Jupiter (Germany) was used for both the TG and DSC tests simultaneously. At a constant heating rate of 10 °C/min, powdered specimens were heated from 20°C to 800°C in an inert nitrogen environment to collect the DSC and TG spectra. The derivative thermogravimetry (DTG) technique was used to find the exothermic and endothermic reaction temperature corresponding to the transformation due to heating. Also, the thermogravimetric technique measured the mass loss due to the decomposition of minerals.

2.4.6. Microstructural investigation

Samples, collected from the top surface (25 mm depth) of LWAC, were used for microstructural analysis. LWAC samples' microstructures at the original condition and after 80 cycles of HC fluids and high-temperature exposures were analysed by Zeiss Axio Imager 2 optical microscope. This machine enabled us to study the microcrack and voids development in the samples. LWAC microstructure was analysed using two main techniques: scanning electron microscope (SEM) and direct observation with an optical microscope. Combining results from both methods allows a better understanding of the morphology of aggregate, interfacial transition zone (ITZ) cracks, composition, microcrack development and propagation.

3. Result and discussion

3.1. Residual mechanical properties

3.1.1. Compressive strength

The residual compressive strength of LWAC samples was tested at an interval of 20 cycles, as shown in Figure 4. For frequent exposure to HC fluids and high temperatures, all samples lost a significant amount of their initial compressive strength. The initial compressive strength of control,

Preprints (www.preprints.org) | NOT PEER-REVIEWED | Posted: 12 December 2023 doi:10.20944/preprints202312.0767.v1

brick and lytag aggregate concrete was in the range of 65-80 MPa. However, the pumice concrete sample and the perlite concrete had a compressive strength of 39 and 22 MPa, respectively. For only high-temperature exposed samples, the control sample lost 33.40 % of the initial compressive strength, similarly, strength loss of 31.20 % and 27.6 % were recorded for brick and lytag specimens. Due to a lower density and stiffness, pumice, and perlite LWAC samples suffered significant strength loss of 48.70 % and 55.80 %, respectively.

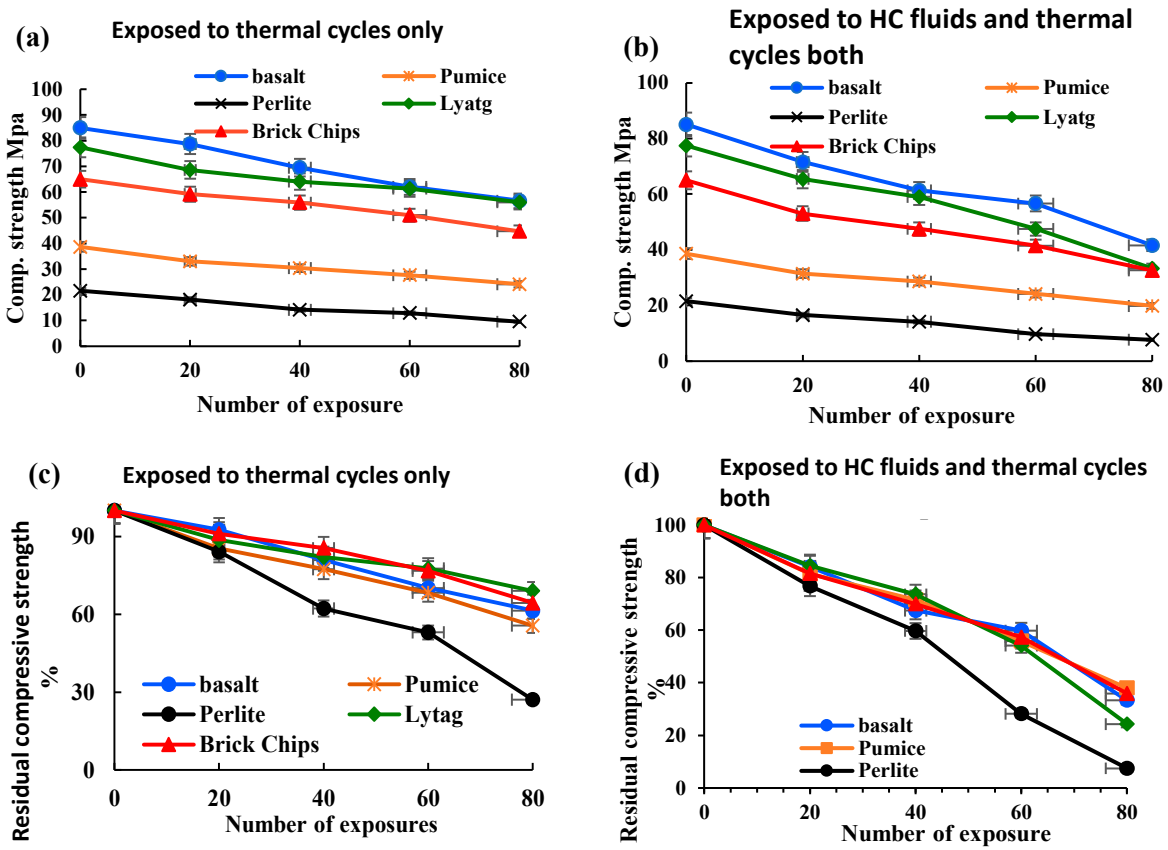

Figure 4. Residual compressive strength (a) High temperature exposed LWAC, (b) HC fluids and high temperature exposed LWAC; % of residual compressive strength retained (c) High temperature exposed samples only, (d) HC fluids and high temperature exposed LWAC samples.

The control sample lost 51.10% of the initial compressive strength for combined HC fluids and high-temperature exposures. Under a similar condition, pumice and brick concrete specimens' strength loss was 48.70 % and 49.80 %, respectively. However, lytag and perlite LWAC samples suffered significantly; they lost 57 % and 64.4 % of initial compressive strength, respectively. The simultaneous effect of HC fluids and thermal cycles is substantially higher than the single effect of high thermal cycles. Also, Most of the LWAC showed a lower residual compressive strength than that of the control concrete. Based on the compressive strength test results, Lytag and brick LWAC performed much better than pumice and perlite LWAC under the combined action of the repeated high-temperature and HC fluids exposures.

3.1.2. Indirect tensile strength

Concrete's tensile strength behaviour indicates its performance under tensile loads and chances of crack formation in members. The indirect tensile strength test was done at 0, 30, 60 and 80 cycles of exposure, as shown in Figure 5. Indirect tensile strength of basalt, brick, lytag, pumice and perlite aggregate concrete at 0 exposure conditions was 5.7, 4.55, 4.22, 3.84, 2.9 MPa, respectively. After 80 cycles of high temperature and HC fluids exposures, the tensile strength loss of basalt, brick, lytag, pumice and perlite concrete were 40.95%, 41.76%, 44%, 55.52%, 22.51%, respectively. The results show

Preprints (www.preprints.org) | NOT PEER-REVIEWED | Posted: 12 December 2023 doi:10.20944/preprints202312.0767.v1

that with the increases in the number of heat exposures, the indirect tensile strength is reduced significantly; it agrees with the previous literature [9].

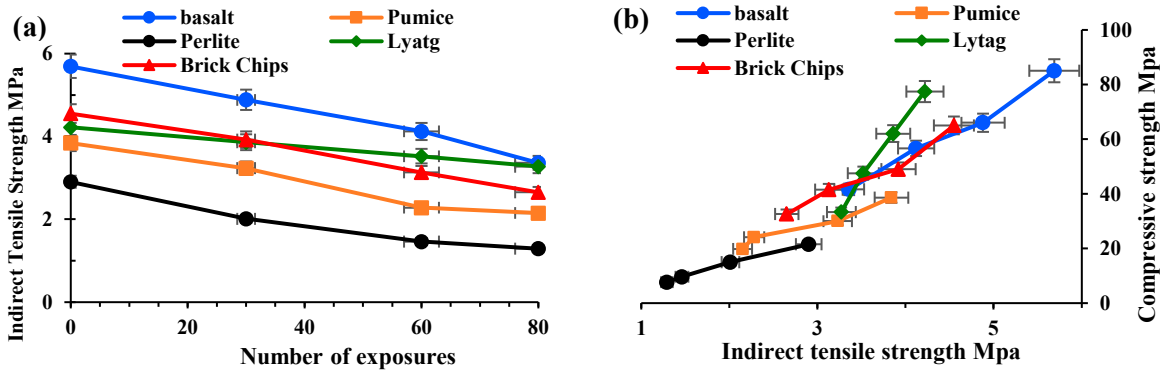

Figure 5. Indirect tensile strength relationship (a) tensile strength vs number of exposures to high-temperature and HC fluids (b) tensile strength vs compressive strength of concrete after exposure.

Figure 5(b) also indicates that both the compressive strength and tensile strength decrease with the increase in high-temperature exposures. However, the decrease in tensile strength is more substantial than the compressive strength reduction. These two strengths are closely related, but there is no direct proportionality between them.

3.1.3. Stress-strain

The stress-strain relationship of LWAC after 0, 30 and 80 cycles of combined HC fluids and high-temperature exposures is shown in Figure 6. The stress-strain curve becomes flattened with the increase in the number of exposures. The peak stresses shift downwards and rightwards because of exposures. These phenomena indicate the peak stress decreases and peak strain increases with the increase of exposure numbers, [9]. Therefore, concrete samples reduced stiffness due to the exposure conditions. Concrete with perlite performed the worst compared to other LWA concrete samples. Concrete made with Lytag showed better resistance to the simulated conditions compared to concrete samples made with other LWA. Moreover, the concrete with crushed brick aggregates showed considerable resistance to the same conditions even after 80 cycles of exposure. Briefly, regardless of the type of aggregates, exposures of concrete to repeated HC fluids and high temperature cause significant loss of compressive strength and an increase in corresponding strain.

Similar to the findings of some other researchers [10, 25], this study also believes that the texture, shape and gradation of LWA directly influenced the stress-strain behaviour of concrete. Besides, the porosity and particle density of aggregates influence the stiffness of concrete, as perlite has higher porosity and lower density, it showed poor performance against the exposure conditions. The reasons for the phenomenon are further investigated by using SEM and optical microscopes and reported later in the paper.

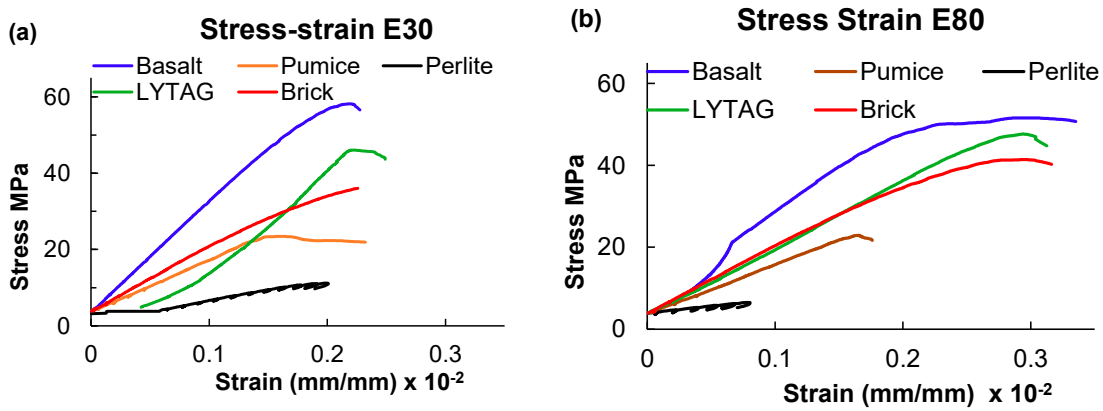

Preprints (www.preprints.org) | NOT PEER-REVIEWED | Posted: 12 December 2023 doi:10.20944/preprints202312.0767.v1

Figure 6. Stress-strain curve of various LWA concrete samples exposed to high-temperature and HC fluids combined (a) After 30 cycles, (b) After 80 cycles.

3.1.4. Concrete Spalling

Some researchers [19, 26, 27] reported that spalling in high-strength concrete occurred when subjected to very high temperatures. Generally, up to 200^{0}C temperature, concrete does not suffer any spalling damage. However, from Figure 7, it is evident that the basalt concrete specimen suffered significant spalling damage due to the recurrent coupled effect of HC fluids and 175^{0}C temperature. After 80 cycles of HC fluids and high-temperature exposures, pumice, perlite, and Lytag specimens also suffered spalling damage but the degree of spalling of LWAC was less than normal concrete. The maximum size of spalling in basalt aggregate was 24.33 mm x 24.49 mm x 5.6 mm. Under a similar condition, brick LWAC showed no spalling damage. Similarly, LWAC samples exposed to 80 cycles of only high temperature exhibited no significant spalling. When exposed to only high temperatures, the dense microstructure of normal-weight concrete (NWC) prevents moisture from escaping, thus causing cracking in concrete. When exposed to the combined effect, HC fluids triggers strength degradation by forming detrimental salts [14, 19] and heat cause the formation of crack; thus, the combined effect of chemicals and high temperature cause the spalling. Overall, LWAC samples did not suffer significant spalling because of their porous microstructures, as vapour pressure was released immediately when heated.

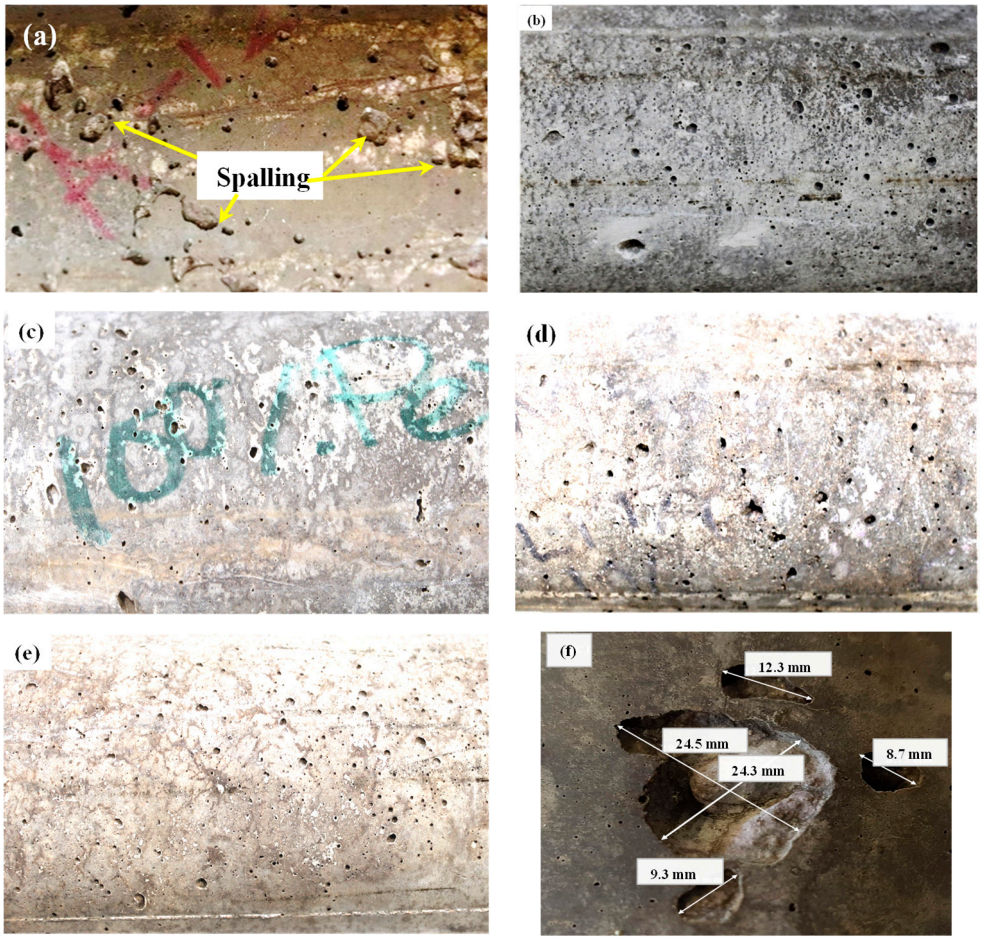

Preprints (www.preprints.org) | NOT PEER-REVIEWED | Posted: 12 December 2023 doi:10.20944/preprints202312.0767.v1

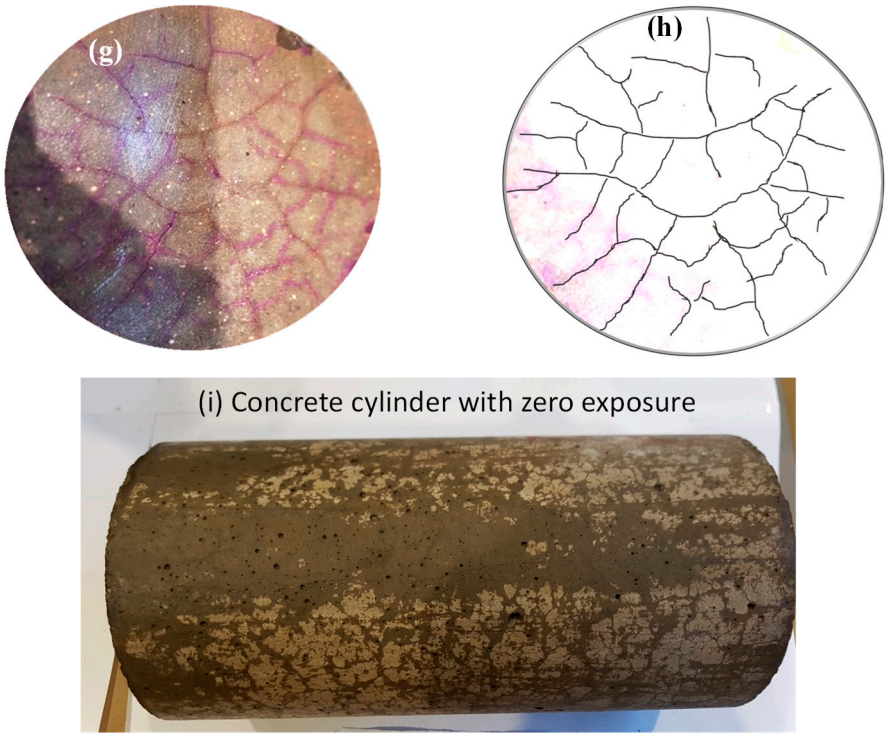

Figure 7. Surface spalling and cracks (a) Control, (b) Pumice, (c) Perlite, (d) LYTAG, and (e) Bricks aggregate concrete, (f) Details of control spalling, (g&h) Surface cracks on control samples, and (i) concrete cylinder with zero exposure.

3.1.5. Mass Loss

Figure 8 shows the mass loss percentage of LWAC samples after exposures. Within the first few cycles, samples lost their initial free water entirely due to frequent high heat exposures. The mass loss curves flattened after 20 cycles of high temperature and HC fluids exposures, suggesting that the concrete matrix lost its initial free water. Maximum water losses of LWAC samples after the first 20 cycles was 19.13%, 11.83%, 7.96 % and 7.31%, respectively, for perlite, pumice, brick and lytag. Pumice and perlite LWACs' water loss was higher because they held more amount of free water due to higher permeability. Khalifa et al. [28] also reported that the concrete segment's permeability between the drying dehydrating front and the heated face controls the mass loss kinetics. For normal-weight aggregates (NWA), such as basalt, having higher density and lesser porosity hold less pore water, thus releasing only 2.87% of water due to heating.

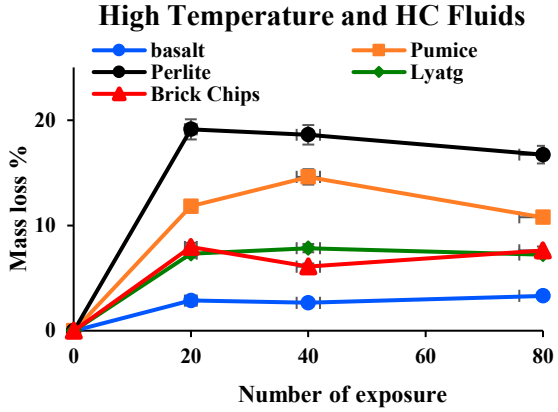

Figure 8. LWAC samples mass losses after exposures to repeated HC fluids and high temperature.

Preprints (www.preprints.org) | NOT PEER-REVIEWED | Posted: 12 December 2023 doi:10.20944/preprints202312.0767.v1

Due to repeated exposure to 175^{0}C temperature, extra water evaporation occurs; when this free water is lost, mass loss continues due to decomposition of cement elements and release of chemically bound water. After 80 cycles of exposures, the mass loss for basalt, pumice, perlite, lytag and brick was 3.71%, 4.44%, 7.72%, 4.98% and 3.95%, respectively. As the mass loss could have been due to the decomposition of mineral compounds in concrete. Therefore, the mass loss phenomenon due to cement elements' decomposition was further investigated by TG analysis later in the paper.

3.2. Thermo-mechanical properties

3.2.1. Thermal conductivity

Thermal properties of concrete depend on many factors, including material mix proportion, types of aggregate, aggregate structure, density, porosity and degree of crystallisation [29, 30]. At ambient temperature, the thermal conductivity of NWC is reported to be in the range of 1.4 - 3.6 W/m.K, and it changes with an increase/decrease in temperature [31]. LWAC shows lower thermal conductivity due to its high porosity and entrapped air's low thermal conductivity. Thus, replacing NWA with LWA affects concrete porosity and its thermal conductivity [32]. Figure 9 shows the thermal conductivity of LWAC subjected to high temperature only and simultaneously exposed to high temperature and HC fluids. Samples thermal conductivity was measured at 30^{0}C at different exposure conditions like after 0, 40 and 80 cycles exposures.

The thermal conductivity of basalt, lytag, brick, pumice and perlite aggregate concrete were 2.02, 1.72, 1.24, 1.11 and 0.95 W/m.k, respectively. From the varying initial thermal conductivity values, it is understood that variation in aggregate structure, porosity and crystallinity affects their thermal conductivity. Thermal conductivity for basalt, lytag, brick, pumice and perlite LWAC samples after 80 cycles of high-temperature exposures were 0.73, 1.03, 0.56, 0.67 and 0.59 W/m.k, respectively. With an increase in high temperature and HC fluid exposures, the thermal conductivity of concrete reduces gradually. Basalt and brick aggregate concrete suffered 63.91% and 54.68% loss of thermal conductivity after 80 cycles, whereas other LWAC suffered 37%-40.12% loss only from original conditions.

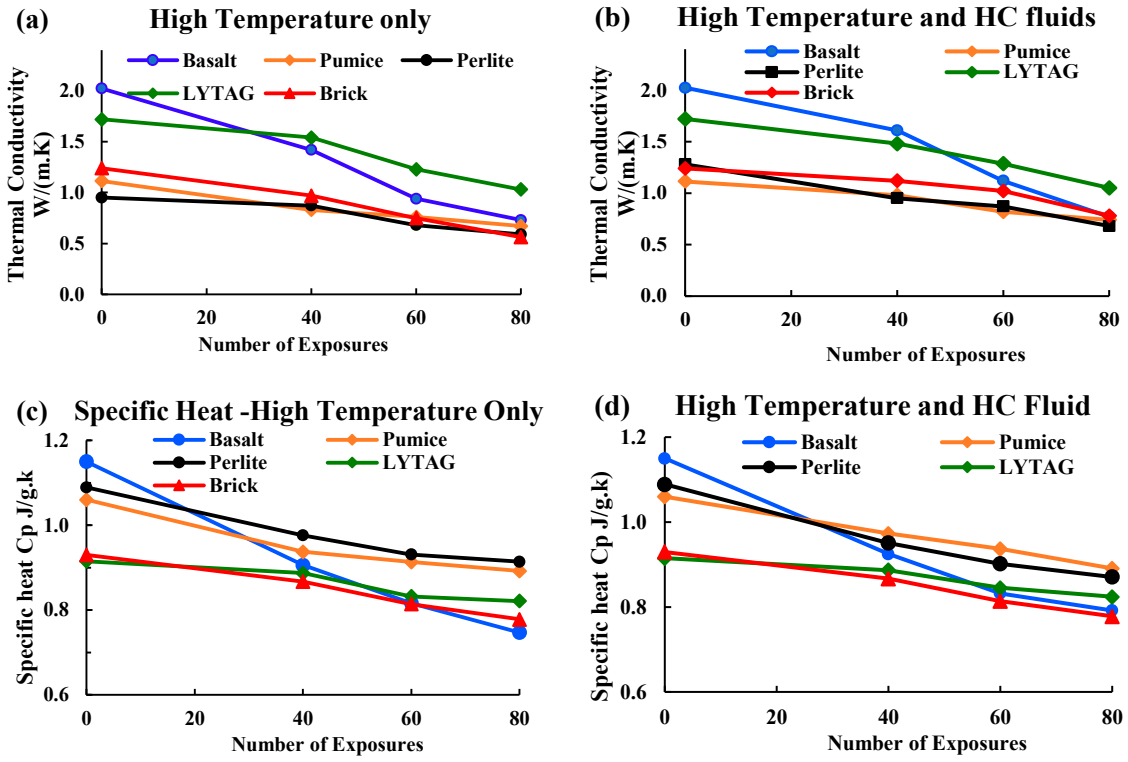

 doi:10.20944/preprints202312.0767.v1

Figure 9. (a) Thermal conductivity of only heat-exposed samples, (b) Thermal conductivity of HC fluids and heat-exposed samples, (c) Specific heat of heat-exposed samples, (d) Specific heat of HC fluids and heat-exposed samples.

In summary, the basalt aggregate's thermal conductivity value was much higher than the LWAs. This may be due to dense microstructure and higher crystallisation of NWA concrete. Due to repeated exposures to the coupled effect of HC fluids and high temperature, these samples had higher thermal conductivity than other samples. Because fluid exposure increases the pore water, which is thermally more conductive than pore air. In all concrete samples, thermal conductivity decreased significantly with increased exposures due to crack growth and propagation.

3.2.2. Specific Heat

Higher specific heat of concrete helps to increase its temperature stability. Usually, the specific heat of different concrete aggregates at ambient temperature varies between 0.84 to 1.8 J/g·K. LWAC samples tested during this test had initial specific heat between 0.92-1.2 J/g.K. Various physical and chemical transformations at higher temperatures directly influence LWAC samples' heat properties. TG analysis (section 3.3.3) shows that at about 150^{0}C, concrete lost almost all free water and crack development started, influencing heat properties. Figure 9 illustrates the variation of specific heat of basalt and LWAC samples exposed to high temperature only and combined exposure to the high temperature and HC fluids.

The graph shows that initially, basalt aggregate has higher specific heat than other LWAC samples. With an increase in the number of exposures to the combined effect of high temperature and HC fluids, the specific heat reduces gradually, especially for basalt aggregate. Though basalt, pumice, and perlite aggregate concrete had almost similar specific heat, after 80 cycles of high-temperature exposures, basalt concrete's specific heat reduced by 35%, whereas other LWA concrete lost around 10-16% only, as shown in Table 3. After 80 cycles of HC fluids and high-temperature exposures, basalt, pumice, perlite, lytag and brick aggregate concrete samples, specific heat reduction was 31.13%, 15.94%%, 20.01%, 9.94% and 10.26%, respectively.

Table 3. Loss of % of thermal conductivity and specific heat after 80 cycles of HC fluids and high temperature exposures.

Types/Loss	Thermal conductivity %		Specific heat %	
	Heat exposed	HC and heat exposed	Heat exposed	HC and heat exposed
Basalt	63.91	61.94	35.04	31.13
Brick	54.68	37.09	16.34	10.26
Lytag	40.12	38.97	7.44	9.94
Pumice	39.86	33.57	15.85	15.94
Perlite	37.96	46.87	16.07	20.01

In brief, in the original condition, LWAC has lower thermal conductivity than NWC, but after 80 cycles of high-temperature exposures, LWA's specific heat was higher than basalt aggregate. It implies that LWA shows much stable behaviour to high-temperature exposures than basalt. Nevertheless, considering mechanical strength and thermal properties, brick aggregates will be more suitable for concrete uses that need higher mechanical strength and good thermal properties.

3.3. Thermochemical properties

3.3.1. FTIR spectrums of HC fluids

Preprints (www.preprints.org) | NOT PEER-REVIEWED | Posted: 12 December 2023 doi:10.20944/preprints202312.0767.v1

Figure 10 represent the FTIR spectrum of HC fluids used in this experiment which is primarily made by mixing jet fuel, hydraulic fluids, and engine lubricating oil in equal proportion. The C-H bond's stretching vibration was represented by three prominent peaks at 2956, 2923 and 2854 cm^{-1}, which dictates alkanes' presence [13]. The ester of fatty acids represented by the stretching vibration of the C=O bond was detected with a major peak at a wavenumber of 1742 cm^{-1} [13]. In the fingerprint region, medium to weak peaks at a wavenumber of 1465, 1378 and 731 cm^{-1} represent the aromatics alkenes, $-CH_2-$, $-CH_3-$ representing the bending vibration of the C-H bond [13]. Peaks at 1156, 1107 and 1022 cm^{-1} dictate the P=O bond of phosphonate, phosphate ester/phosphoric acids [33, 34].

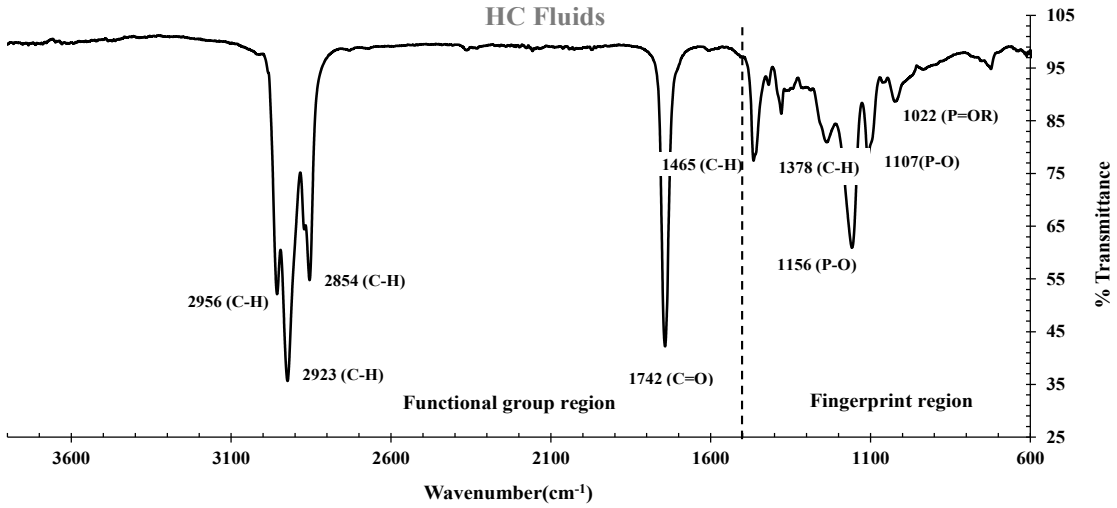

Figure 10. The FTIR spectrum of hydrocarbon fluids used.

Based on the FTIR analysis of HC fluids used in this experiment, the phosphonate, phosphine oxide, phosphate and esters of fatty acids were identified as part of lubricating oils. Similarly, free alcohol/phenol, alkanes, phosphate esters and esters of fatty acids were present in the hydraulic fluid. This oil also contains long-chain hydrocarbons of $-CH_3-$, $-CH_2-$, alkenes and aromatic compounds.

3.3.2. FTIR analysis of LWAC samples

Control concrete specimen FTIR spectrum shows sulphate, silicate, carbonate and hydroxide peaks [35]. Figure 11(a) shows an FTIR spectrum of the control specimen at the original condition, after 40 & 80 HC fluids and high-temperature exposures and 80 cycles of high-temperature exposures only. A small broad pick denotes chemically bound water for H-OH bonds' stretching vibration at wavenumber 2968 cm^{-1}. The carbon dioxide is represented by the stretching mode of C=O by a small weak peak at a wavenumber of 2358 cm^{-1} [36]. The presence of limestone from Portland cement is symbolised by the stretching mode of the C-O bond detected by a broad medium peak at wavenumber 1365 cm^{-1} and 780 cm^{-1} [35]. Calcium sulphate is represented by the stretching mode of the S=O bond detected at a wavenumber of 1216 cm^{-1} [35, 37]. C-S-H gel and related silicate paste represented by the Si-O bond are seen at a noticeable broad peak of 1005 cm^{-1} [35, 38]. Finally, the quartz components' crystalline phase was detected at the peaks at 693 and 646 cm^{-1} [13].

Significant changes were observed in pumice and perlite at 0 and 80 cycles in peak height, shifting of position or altogether disappearance due to repeated exposure to high temperature and HC fluids. Figure 12(a) second and thirds spectrum show FTIR spectrum of basalt concrete exposed to high temperature and HC fluids after 40 and 80 cycles. It was noticed that due to repeated high temperature and HC fluids exposures, the basalt concrete peak for hydroxyl ion (-OH) of $Ca(OH)_2$ was destroyed by the chemical compounds of HC fluids. The alkanes related C-H bonds' stretching vibration was detected at 2981 & 2883 cm^{-1} [13]. Usually, ordinary cement does not contain any alkanes molecules; HC fluids contributed alkanes. Changes are observed in the silicate absorbance bands in the 1200–800 cm^{-1} wavenumber region [13].

Preprints (www.preprints.org) | NOT PEER-REVIEWED | Posted: 12 December 2023 doi:10.20944/preprints202312.0767.v1

No peaks for the esters of fatty acids were detected in the basalt concrete cylinders. Calcium salt was produced due to a chemical reaction between calcium hydroxide and fatty acid [13]. Similarly, as seen in Figure 12, after 80 cycles of high-temperature exposures of pumice, perlite and lytag LWAC, peaks at 1216,1365, and 1735 cm^{-1} are still available; due to non-exposures to HC fluids, so they are not consumed by alkanes or ester of HC fluids. Only dehydration of concrete occurs in high temperatures exposed samples.

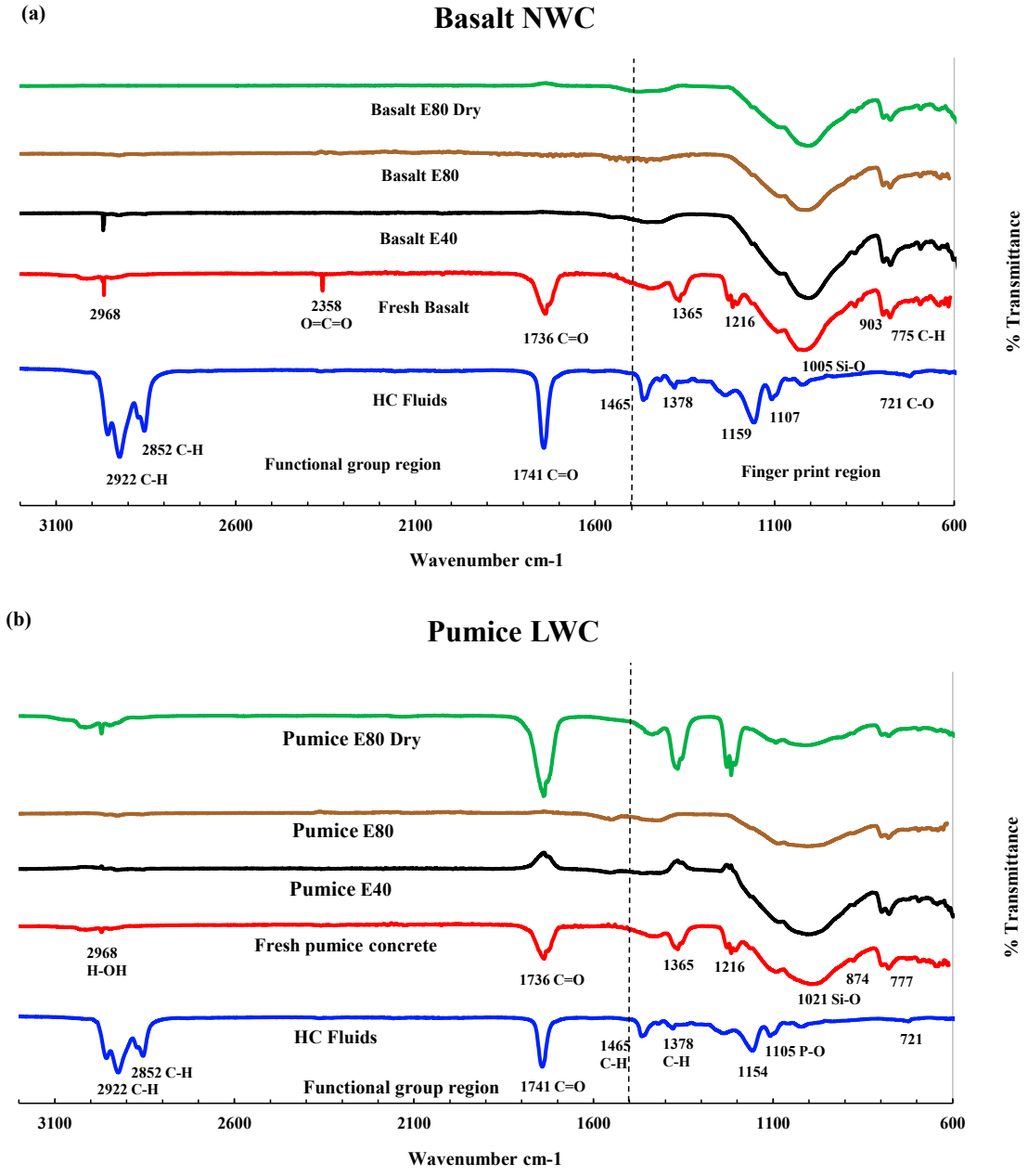

Figure 11. FTIR analysis (a) Basalt NWC, (b) Pumice LWAC.

Preprints (www.preprints.org) | NOT PEER-REVIEWED | Posted: 12 December 2023 doi:10.20944/preprints202312.0767.v1

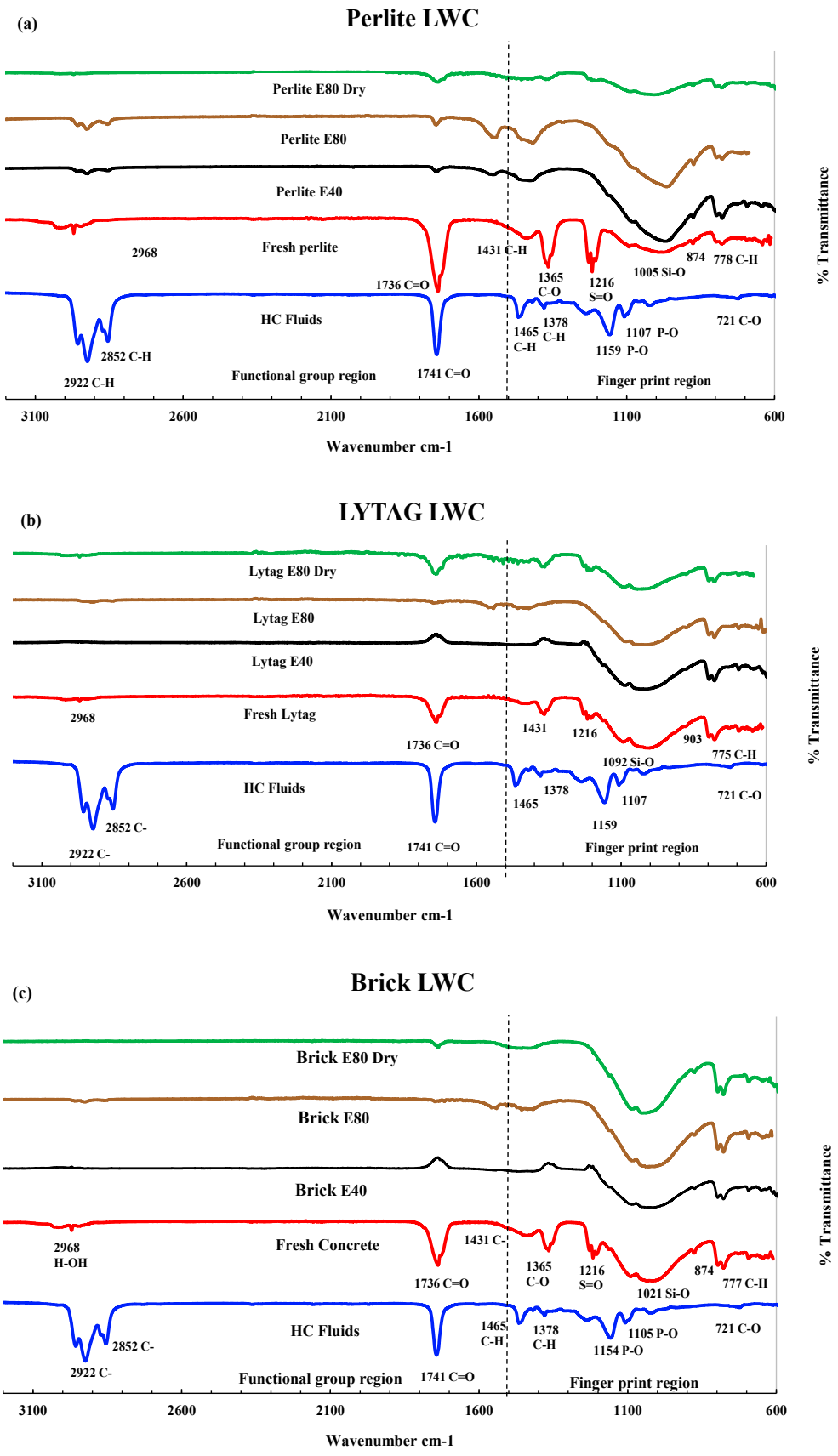

Figure 12. FTIR analysis (a) Perlite LWA concrete, (b) Lytag LWA concrete and (c) Brick LWAC.

3.3.3. Thermogravimetric analysis

Preprints (www.preprints.org) | NOT PEER-REVIEWED | Posted: 12 December 2023 doi:10.20944/preprints202312.0767.v1

Figure 13 shows the thermogravimetric (TG) test result for LWAC samples exposed to recurrent HC fluid and high temperature. The TG curve of the original concrete showed three rapid weight-loss sections. The picks between 20 to 200°C represent weight losses due to the evaporation of parts of the bound water and free water; Fares et al. [39] also reported that the free water was eliminated at 120°C. Gypsum starts decomposing at 182°C along with ettringite [40], and carboaluminate hydrates and causes mass loss. This sharp mass loss between the 30°C-200°C temperature range was evaluated to be about 3.19%, 7.04%, 9.84%, 6.67% and 4.93%, respectively, for Basalt 0, Pumice 0, Perlite 0, lytag 0 and Brick 0. Repeated exposure to HC fluid and high-temperature cycles caused a reduction in mass loss. After initial exposure, excess and bound water almost dries up. With the increase in high-temperature exposures, the mass loss above 600°C temperature increases, as seen in Table 4.

The DTG graph shows that after the initial rapid decline, the second weight loss in the range of 200^{0}C – 350^{0}C was due to C-S-H gel decomposition and bound water release. The most significant weight loss is observed between 350–600^{0}C temperature, where portlandite starts disintegrating until completion of the process at around 480^{0}C. [41]. The mass loss after 80 cycles was 10.95%, 5.94%, 5.04% and 4.8% in perlite, pumice, lytag and brick, respectively. This significantly higher value is only observed in HC fluids exposed samples only, which may be due to cement compounds' chemical reaction with the element of aviation oils. However, after 400^{0}C, mass loss was significantly higher for ordinary concrete control specimens than LWAC samples. In the range of 700–800^{0}C, the mass loss was due to the decomposition of C-S-H (II) into wollastonite and larnite and the release of carbon dioxide, which accounts for 4.75%, 7.14%, 3.9% and 3.39% of mass loss in pumice, perlite, lytag and brick 80 cycles samples, respectively.

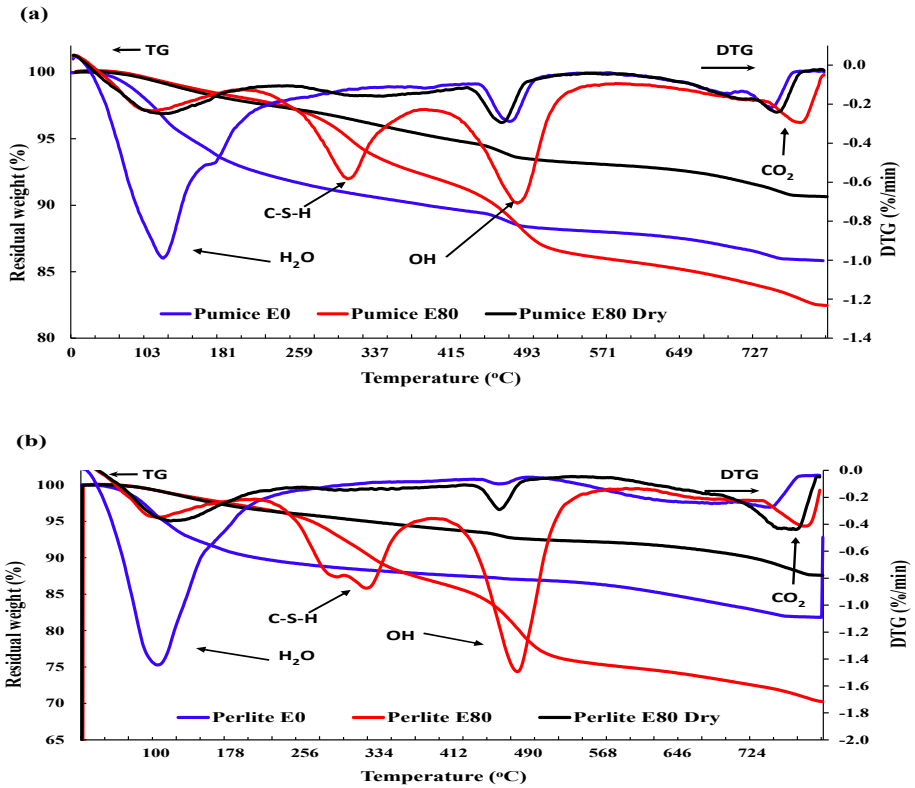

Preprints (www.preprints.org) | NOT PEER-REVIEWED | Posted: 12 December 2023 doi:10.20944/preprints202312.0767.v1

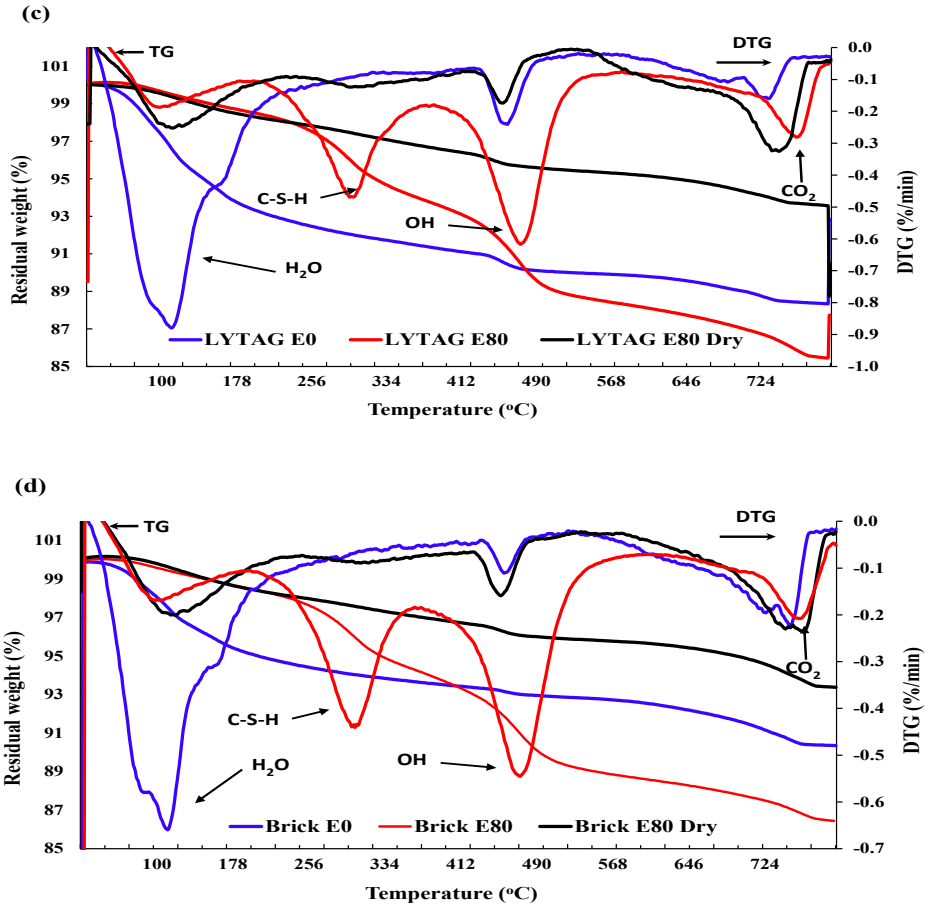

Figure 13. TG and DTG analysis of LWAC exposed to HC fluids and high temperature. (a) Pumice, (b) Perlite, (c) Lytag, (d) Brick.

Table 4. Loss of thermal conductivity and specific heat after repeated exposures.

Aggregates	Mass loss in the various temperature range			
	20-200°C	200-350°C	350-600°C	600-800°C
Pumice E0	7.04	2.45	2.12	2.5
Pumice E80	1.94	4.91	5.94	4.75
Pumice E80 Dry	2.14	1.99	2.39	2.77
Perlite E0	9.84	2.08	1.14	5.11
Perlite E80	3.04	8.6	10.95	7.14
Perlite E80 Dry	3.17	2.12	2.09	4.87
LYTAG E0	6.67	1.71	1.53	1.76
LYTAG E80	1.47	4.13	5.04	3.9
LYTAG E80 Dry	1.72	1.33	1.4	1.97
Brick E0	4.93	1.31	0.93	2.57
Brick E80	1.49	3.88	4.8	3.39
Brick E80 Dry	1.56	1.25	1.22	2.59
Basalt E0	3.19	0.82	1.13	2.03
Bsalt E80	2.92	2.5	3.17	3.64

Preprints (www.preprints.org) | NOT PEER-REVIEWED | Posted: 12 December 2023 doi:10.20944/preprints202312.0767.v1

In brief, the porous microstructure of pumice and perlite has allowed more absorption of pore water. Thus, repeated exposures to high temperature and HC fluids pumice and perlite aggregate suffered more mass loss than brick and lytag aggregate.

3.3.4. DSC Analysis

In DSC analysis of LWAC samples repeatedly exposed to high-temperature and HC fluid, we observed four distinct exothermic peaks at 30°C-150 °C, 400°C-500°C, 550°C-570°C and 700°C-750°C as shown in Figure 14. Between 50–150°C temperature, the double peaks indicated significant mass loss due to the partial loss of evaporable water and chemically bond water from C–S–H gel and ettringite hydrates [13]. Between 100–300°C temperature range, rapid water migration caused the micro-cracks in specimens, triggering the residual compressive strength's rapid degradation.

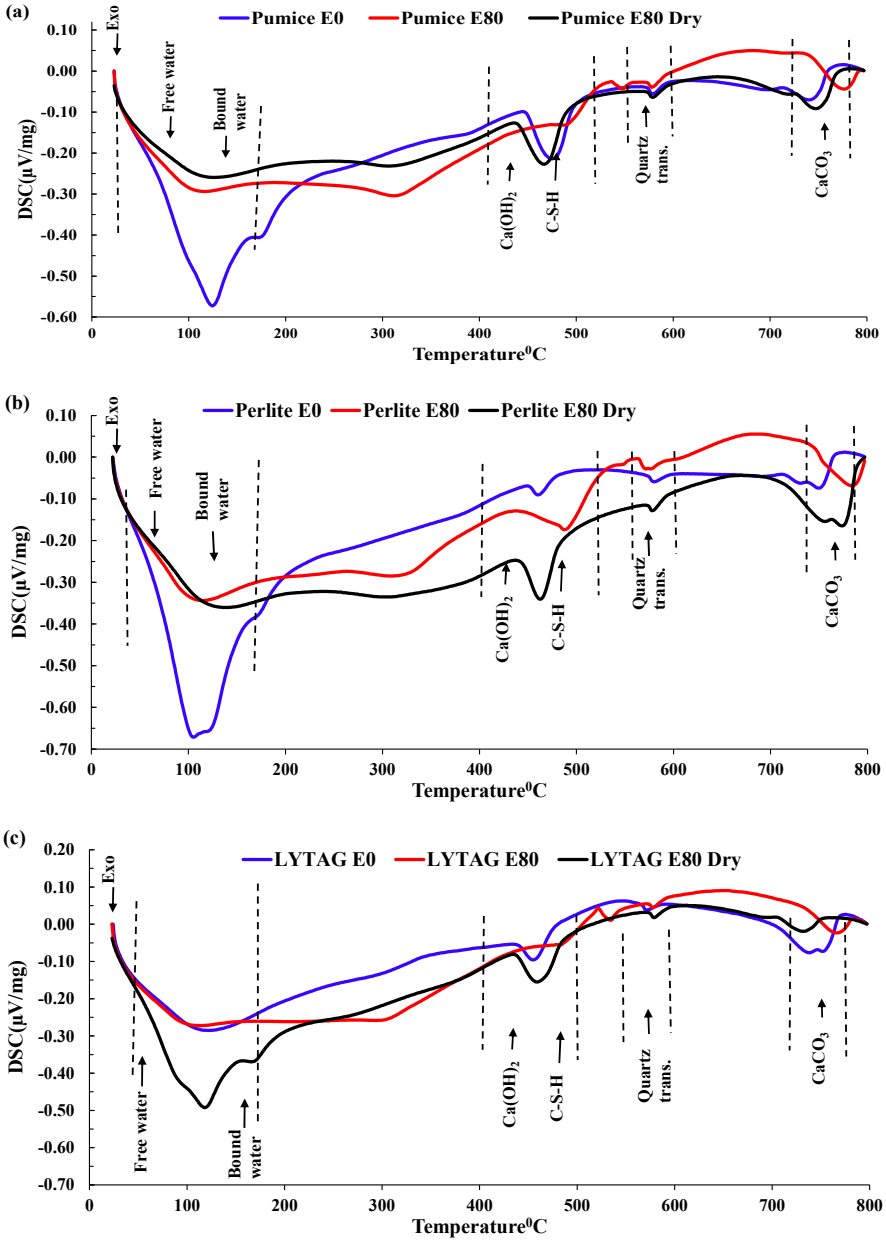

Preprints (www.preprints.org) | NOT PEER-REVIEWED | Posted: 12 December 2023 doi:10.20944/preprints202312.0767.v1

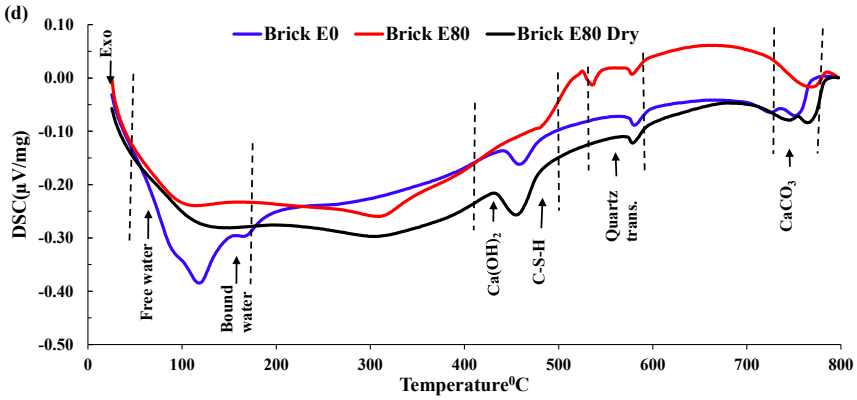

Figure 14. DSC of high temperature and HC fluid exposed LWAC (a) Pumice, (b) Perlite, (c) Lytag and (d) Brick samples.

According to Khoury [42], the continuous dehydration of C–S–H between 200⁰ C and 300 °C caused a slight variation of heat flow in this range. However, several other researchers [43] reported that the breakdown of tobermorite gel and water loss from pores of hydrates caused heat flow variation between 200⁰ C and 400° C temperature range. Around 430⁰C- 450°C, portlandite decomposed into free lime (dehydroxylation) with a significant peak. At 573 °C, the solid-state phase transformation of quartz-α into quartz-β occurs with an enlargement/cracking in some coarse aggregates. Similar to previous findings, we also detected the decomposition of C-S-H gel and the formation of β-C_2S between 600°C -700 °C. Between 700 °C -800 °C in the exothermic phase, the decomposition of the $CaCO_3$ caused the release of CO_2 [33, 42], although insignificant mass loss occurred. Repeated exposures to HC fluids and higher temperatures caused some phases' partial or total disintegration because several peaks' disappeared or reduced/shifted to a higher temperature. Samples with higher porosity like pumice and perlite have higher peaks and give up more water in the initial temperature range.

In brief, between 100°C –300 °C temperature range, rapid water migration develops micro-cracks in specimens, leading to the rapid degradation in residual compressive strength. DSC confirms that evaporable and chemically bound water was jettisoned gradually according to their binding forces. The evaporation of free and bound water caused an increase in the concrete's porosity. These chemical and physical changes resulted in changing the LWAC samples' residual mechanical properties and thermal properties.

3.4. Morphology and microcracks-voids

3.4.1. Morphology of aggregates

Figure 15 shows the micrographs of the lytag, perlite and brick LWA concrete obtained using SEM. The microstructure of the various LWA had a significant difference between them. The microstructure of basalt, brick, pumice, lytag and perlite aggregates varies from solid to porous and significantly affects thermal and mechanical properties, as seen in previous sections. The diameter of the pores of LWA varied from 10-70µm. Generally, the pores inside the LWA were independent of each other and separated from the outer surface; however, the perlite aggregate pores were connected to outer surfaces. Additionally, SEM images revealed that LWA surface morphology was uneven, unlike the NWA; thus, better bonding between the aggregate and cement past occurred and improved the mechanical interlocking action.

Preprints (www.preprints.org) | NOT PEER-REVIEWED | Posted: 12 December 2023 doi:10.20944/preprints202312.0767.v1

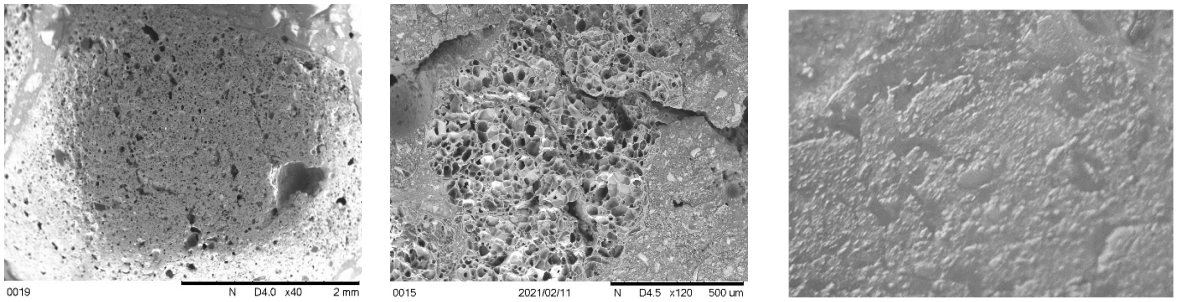

Figure 15. Morphology of different LWA (a) Lytag, (b) perlite, and (c) brick.

3.4.2. ITZ, microcracks and voids

SEM and optical microscopic investigation were carried out after 0 and 80 cycles of recurrent HC fluids and high-temperature exposure for effect on ITZ, types of aggregate, and hydration of cement paste. Due to significant differences in the morphology of LWA, the boundary between LWA and cement paste can be distinguished. LWA shown in the above, is characterised as having a porous interior structure. Clear-cut thermal cracks between aggregate and cement paste were found in basalt, pumice and brick aggregate. By magnifying the ITZ between aggregate and cement paste by 2.5 k, as shown in Figure 16(a), the thermal crack measured to be approximately 3 μm. Moreover, by SEM micrograph, we found that LWAC bonding between the cement paste and aggregate is much better than NWA and cement paste [44].

Basalt aggregates in NWC act as a barrier to thermal microcracks propagation and allow it to spread along with the cement paste-aggregate interface. Moreover, microcracks in LWA start from cement paste then pass through the ITZ into the weak, porous lightweight aggregate. Thus, microcrack propagation helped us to understand the LWA failure mechanism. Like these, thermal cracks develop due to thermal stress development, and the number of cracks increases with the increase in high-temperature exposures. Thermal cracks in perlite aggregate did not follow ITZ; instead, they followed a weak and porous zone [Figure 17(b)].

Furthermore, due to the increase in high-temperature exposure, the quantity and extent of thermal cracks increase. A significant increase in air voids was observed in basalt and brick aggregate concrete samples due to aggregate non-porosity. Due to repeated heating and HC fluid exposure, the ejection of water/HC fluid vapour creates numerous irregular air voids, which allow the penetration of HC fluids. The destructive effect of vapour pressure during high temperature exposure is evident in the form of cracks within the porous aggregates.

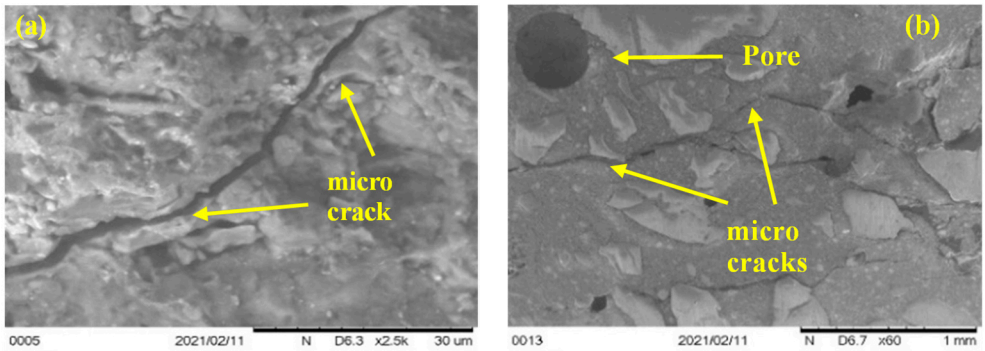

Preprints (www.preprints.org) | NOT PEER-REVIEWED | Posted: 12 December 2023 doi:10.20944/preprints202312.0767.v1

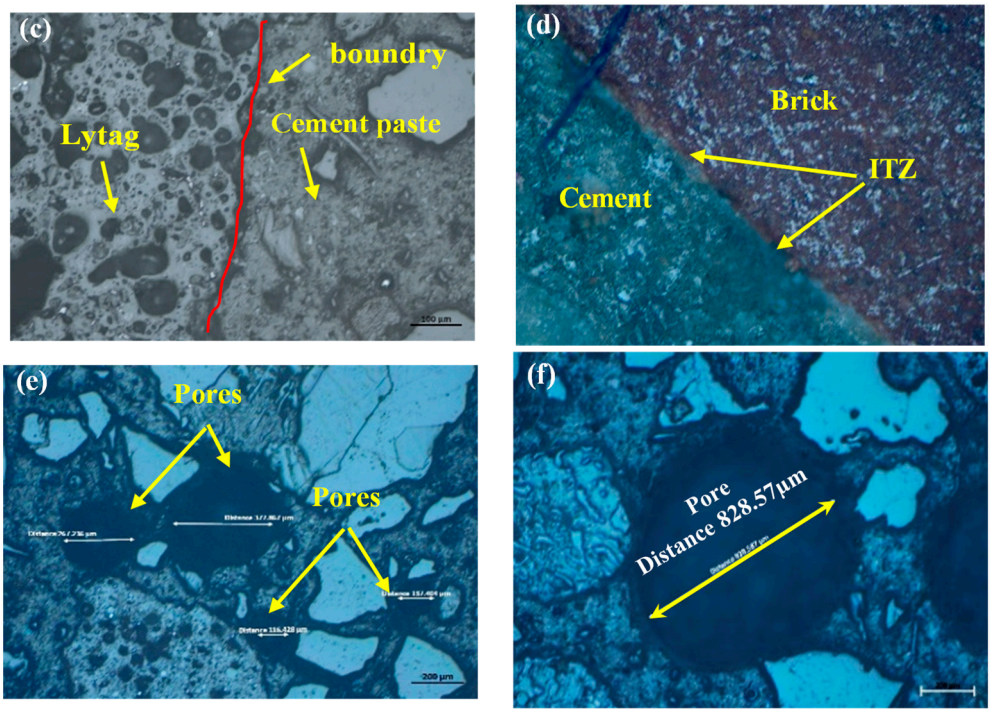

Figure 16. ITZ SEM micrographs for LWAC and NWC: (a) Brick sample microcrack (×2.5k), (b) Multiple cracks in pumice aggregate (x60), (c) ITZ between LYTAG and cement paste (x20), (d) ITZ between brick and cement paste (x20), (e) Multiple pores in pumice concrete, and (f) Large irregular pore in basalt concrete.

The thermal crack analysis indicated that it follows the weakest zone in the concrete matrix. If the concrete is made of a lightweight (porous) aggregate, concrete releases water vapour through the porosity of aggregates and results in minor or no crack. In NWC, due to the aggregate's dense and sturdy microstructure, the thermal crack follows the ITZ between the aggregate-cement paste.

4. Conclusion and recommendation

This study revealed the resistance of various types of LWAC to a simulated airfield condition. Residual mechanical properties, thermal, chemical, and microstructural properties of LWAC were investigated after repeated exposures to the simultaneous effect of high temperature and chemicals. The following key conclusions can be drawn from the experimental study conducted:

- LWAC retained a moderate amount of residual mechanical strengths after being exposed to repeated high temperatures and HC fluids. After 80 cycles of exposure to the coupled effect of HC fluids and high temperature, both control and LWAC suffered a significant strength loss. Lytag and brick LWAC showed higher compressive strength compared to other LWAC types and retained a residual compressive strength like the control specimen.
- The thermophysical properties of concrete are directly linked with the type and strength of the aggregate of concrete. LWAC showed much better thermal performances than NWA concrete under the repeated actions of HC fluids and high temperatures. Among the LWAC specimens used, perlite and pumice concrete specimens had better thermal performances than lytag and brick aggregate concrete samples due to their porous microstructure.
- Mass loss was prominent for pumice and perlite aggregate concrete due to their higher percentage of porosity. TG and DSC tests showed that the decomposition of cement causes the evaporation of bound water, increasing the mass loss substantially.
- Concrete samples exposed to the coupled effect of HC fluids and high temperature suffered spalling damage. Basalt concrete (control) was detected to develop significant spalling, but pumice, perlite and lytag LWAC suffered relatively less spalling. However, crushed brick concrete showed no spalling damage under the same exposure conditions.

- SEM scans revealed that the low porosity in basalt aggregate caused the cracking in the cement paste at elevated temperatures as vapour pressure was not able to release immediately. Therefore, basalt concrete experienced higher heat-induced microcracks than other LWAC tested.

In brief, LWA types impact the residual thermo-mechanical properties of concrete. Based on the residual mechanical strength and thermal properties, brick LWAC seems to be a promising material for reducing surface spalling of airfields' rigid pavements. For further study, concrete samples can be exposed to one-direction (1D) heating as it happens under the APU exhaust.

Acknowledgments: A research grant from the Australian Defence Force supported the research. The UNSW Canberra laboratories were used for the reported experiments.

Conflicts of Interest: The work published in this paper has no known competing financial interest or personal relationship to the authors that could appear to influence the outcome.

References

1. H. Al-Khaiat, M. Haque, Effect of initial curing on early strength and physical properties of a lightweight concrete, Cement and Concrete Research 28(6) (1998) 859-866.
2. S. Hachemi, A. Ounis, Performance of concrete containing crushed brick aggregate exposed to different fire temperatures, European Journal of Environmental and Civil Engineering 19(7) (2015) 805-824.
3. S. Demirdag, L. Gunduz, Strength properties of volcanic slag aggregate lightweight concrete for high performance masonry units, Construction and building materials 22(3) (2008) 135-142.
4. N.U. Kockal, T. Ozturan, Durability of lightweight concretes with lightweight fly ash aggregates, Construction and Building Materials 25(3) (2011) 1430-1438.
5. K.M.A. Hossain, Properties of volcanic pumice based cement and lightweight concrete, Cement and concrete research 34(2) (2004) 283-291.
6. R. Demirboğa, İ. Örüng, R. Gül, Effects of expanded perlite aggregate and mineral admixtures on the compressive strength of low-density concretes, Cement and Concrete Research 31(11) (2001) 1627-1632.
7. C.-S. Poon, S. Azhar, M. Anson, Y.-L. Wong, Performance of metakaolin concrete at elevated temperatures, Cement and Concrete Composites 25(1) (2003) 83-89.
8. U. Schneider, Concrete at high temperatures—a general review, Fire safety journal 13(1) (1988) 55-68.
9. I. Hager, T. Tracz, J. Śliwiński, K. Krzemień, The influence of aggregate type on the physical and mechanical properties of high-performance concrete subjected to high temperature, Fire and materials 40(5) (2016) 668-682.
10. S. Yehia, M. AlHamaydeh, S. Farrag, High-strength lightweight SCC matrix with partial normal-weight coarse-aggregate replacement: Strength and durability evaluations, Journal of Materials in Civil Engineering 26(11) (2014) 04014086.
11. S.K. Shill, S. Al-Deen, M. Ashraf, Concrete durability issues due to temperature effects and aviation oil spillage at military airbase–A comprehensive review, Construction and Building Materials 160 (2018) 240-251.
12. S.K. Shill, S. Al-Deen, M. Ashraf, W. Hutchison, Resistance of fly ash based geopolymer mortar to both chemicals and high thermal cycles simultaneously, Construction and Building Materials 239 (2020) 117886.
13. S.K. Shill, S. Al-Deen, M. Ashraf, Saponification and scaling in ordinary concrete exposed to hydrocarbon fluids and high temperature at military airbases, Construction and Building Materials 215 (2019) 765-776.
14. S.K. Shill, S. Al-Deen, M. Ashraf, M.M. Hossain, Residual properties of conventional concrete repetitively exposed to high thermal shocks and hydrocarbon fluids, Construction and Building Materials 252 (2020) 119072.
15. S.K. Shill, S. Al-Deen, M. Ashraf, W. Hutchison, M.M. Hossain, Performance of amine cured epoxy and silica fume modified cement mortar under military airbase operating conditions, Construction and Building Materials 232 (2020) 117280.
16. S.K. Shill, S. Al-Deen, M. Ashraf, M.A. Elahi, M. Subhani, W. Hutchison, A comparative study on the performance of cementitious composites resilient to airfield conditions, Construction and Building Materials 282 (2021) 122709.
17. M.C. McVay, L.D. Smithson, C. Manzione, Chemical damage to airfield concrete aprons from heat and oils, Materials Journal 90(3) (1993) 253-258.
18. S.K. Shill, S. Al-Deen, M. Ashraf, M. Rashed, W. Hutchison, Consequences of aircraft operating conditions at military airbases: degradation of ordinary mortar and resistance mechanism of acrylic and silica fume modified cement mortar, Road Materials and Pavement Design (2020) 1-14.
19. M.M. Hossain, S. Al-Deen, M.K. Hassan, S.K. Shill, M.A. Kader, W. Hutchison, Mechanical and thermal properties of hybrid fibre-reinforced concrete exposed to recurrent high temperature and aviation oil, Materials 14(11) (2021) 2725.

20. M. McVay, J. Rish III, C. Sakezles, S. Mohseen, C. Beatty, Cements resistant to synthetic oil, hydraulic fluid, and elevated temperature environments, Materials Journal 92(2) (1995) 155-163.
21. A.F. Bingöl, R. Gül, Compressive strength of lightweight aggregate concrete exposed to high temperatures, CSIR (2004).
22. A. Standard, AS 3972 General Purpose and Blended Cements, (2010).
23. S.J.M.o.T.C. Australian, AS 1010.9-1999: Determination of the compressive strength of concrete specimens, (1999).
24. C. ASTM, 518, Standard Test Method for Steady-State Thermal Transmission Properties by Means of the Heat Flow Meter Apparatus, Annual Book of ASTM Standards (2003).
25. M. Shannag, Characteristics of lightweight concrete containing mineral admixtures, Construction and Building Materials 25(2) (2011) 658-662.
26. S.Y.N. Chan, G.-F. Peng, M. Anson, Fire behavior of high-performance concrete made with silica fume at various moisture contents, Materials Journal 96(3) (1999) 405-409.
27. M.B. Dwaikat, V. Kodur, Hydrothermal model for predicting fire-induced spalling in concrete structural systems, Fire safety journal 44(3) (2009) 425-434.
28. P. Kalifa, G. Chene, C. Galle, High-temperature behaviour of HPC with polypropylene fibres: From spalling to microstructure, Cement and concrete research 31(10) (2001) 1487-1499.
29. H. Oktay, R. Yumrutaş, A. Akpolat, Mechanical and thermophysical properties of lightweight aggregate concretes, Construction and Building Materials 96 (2015) 217-225.
30. A. Tandiroglu, Temperature-dependent thermal conductivity of high strength lightweight raw perlite aggregate concrete, International journal of thermophysics 31(6) (2010) 1195-1211.
31. V. Kodur, M. Sultan, Effect of temperature on thermal properties of high-strength concrete, Journal of materials in civil engineering 15(2) (2003) 101-107.
32. R. Demirboğa, R. Gül, The effects of expanded perlite aggregate, silica fume and fly ash on the thermal conductivity of lightweight concrete, Cement and concrete research 33(5) (2003) 723-727.
33. L. Daasch, D. Smith, Infrared spectra of phosphorus compounds, Analytical chemistry 23(6) (1951) 853-868.
34. Y. Arai, D.L. Sparks, ATR–FTIR spectroscopic investigation on phosphate adsorption mechanisms at the ferrihydrite–water interface, Journal of Colloid and Interface Science 241(2) (2001) 317-326.
35. A. Mendes, W.P. Gates, J.G. Sanjayan, F. Collins, NMR, XRD, IR and synchrotron NEXAFS spectroscopic studies of OPC and OPC/slag cement paste hydrates, Materials and structures 44(10) (2011) 1773-1791.
36. M. Sanati, A. Andersson, DRIFT study of the oxidation and the ammoxidation of toluene over a TiO2 (B)-supported vanadia catalyst, Journal of molecular catalysis 81(1) (1993) 51-62.
37. R. Ylmén, U. Jäglid, B.-M. Steenari, I. Panas, Early hydration and setting of Portland cement monitored by IR, SEM and Vicat techniques, Cement and Concrete Research 39(5) (2009) 433-439.
38. M. Varas, M.A. de Buergo, R. Fort, Natural cement as the precursor of Portland cement: Methodology for its identification, Cement and Concrete Research 35(11) (2005) 2055-2065.
39. H. Fares, S. Remond, A. Noumowé, A. Cousture, Microstructure et propriétés physico-chimiques de bétons autoplaçants chauffés de 20 à 600°C, European Journal of Environmental and Civil Engineering 15(6) (2011) 869-888.
40. L. Alarcon-Ruiz, G. Platret, E. Massieu, A.J.C. Ehrlacher, C. research, The use of thermal analysis in assessing the effect of temperature on a cement paste, Cement and Concrete Research 35(3) (2005) 609-613.
41. R. Way, K. Wille, Effect of heat-induced chemical degradation on the residual mechanical properties of ultrahigh-performance fiber-reinforced concrete, Journal of Materials in Civil Engineering 28(4) (2016) 04015164.
42. G.J.M.o.c.R. Khoury, Compressive strength of concrete at high temperatures: a reassessment, Magazine of Concrete Research 44(161) (1992) 291-309.
43. G. Ye, X. Liu, G. De Schutter, L. Taerwe, P. Vandevelde, Phase distribution and microstructural changes of self-compacting cement paste at elevated temperature, Cement and Concrete Research 37(6) (2007) 978-987.
44. T. Wu, X. Yang, H. Wei, X. Liu, Mechanical properties and microstructure of lightweight aggregate concrete with and without fibers, Construction and Building Materials 199 (2019) 526-539.